JID: FI [m1+;February 20, 2021;4:13]

EI SEVIED

Available online at www.sciencedirect.com

ScienceDirect

Journal of the Franklin Institute xxx (xxxx) xxx



www.elsevier.com/locate/jfranklin

The impact of static output nonlinearities on the control strategies that humans use in command-following tasks[☆]

Sajad Koushkbaghi*, Jesse B. Hoagg, T. Michael Seigler

Department of Mechanical Engineering, University of Kentucky, Lexington, KY, 40506, USA

Received 17 April 2020; received in revised form 11 November 2020; accepted 1 February 2021

Available online xxx

Abstract

The results of a human-in-the-loop experiment are used to investigate the control strategies that humans use to interact with nonlinear dynamic systems. Two groups of human subjects interact with a dynamic system and perform a command-following task. The first group interacts with a linear time-invariant (LTI) dynamic system. The second group interacts with a Wiener system, which consists of the same LTI dynamics cascaded with a static output nonlinearity. Both groups exhibit improved performance over the trials, but the average of the linear group's performance is better on more than three-fourths of the trials. A new nonlinear subsystem identification algorithm is presented and used to identify the feedback and feedforward control strategies used by the subjects in both groups. The identification results for the linear group agree with prior studies suggesting that adaptive feedforward inversion is a primary control strategy used by humans for command-following tasks. The main results of this paper address an open question of whether a similar control strategy is used for nonlinear systems. The identification results for the nonlinear group suggest that those subjects also use adaptive feedforward inversion. However, the static output nonlinearity inhibits the human's ability to approximate the inverse.

© 2021 The Franklin Institute. Published by Elsevier Ltd. All rights reserved.

E-mail addresses: sajad.k@uky.edu (S. Koushkbaghi), jesse.hoagg@uky.edu (J.B. Hoagg), tmseigler@uky.edu (T.M. Seigler).

https://doi.org/10.1016/j.jfranklin.2021.02.007

0016-0032/© 2021 The Franklin Institute. Published by Elsevier Ltd. All rights reserved.

Please cite this article as: S. Koushkbaghi, J.B. Hoagg and T.M. Seigler, The impact of static output nonlinearities on the control strategies that humans use in command-following tasks, Journal of the Franklin Institute, https://doi.org/10.1016/j.jfranklin.2021.02.007

[☆] This work is supported in part by the National Science Foundation (award number: OIA-1849213, CMMI-1405257)

^{*} Corresponding author.

Journal of the Franklin Institute xxx (xxxx) xxx

1. Introduction

Humans are often the least-understood component of a human-in-the-loop (HITL) system. There are many engineering principles and analysis techniques that can be used to predict and design the behavior of dynamic systems, such as aircraft, construction machinery, haptic devices, and telerobotic systems. Predicting how humans will interact with those systems is more challenging. An improved understanding of human control strategies is likely to yield significant advancements in HITL technologies.

Many HITL systems can be modeled using the control architecture shown in Fig. 1. The human interacts with a dynamic system through the control input u, which is generated based on available feedback y and a command signal r. The human's goal is to interact with the dynamic system in a manner that makes the magnitude of the command-following error e = r - y small.

A human's control response is complex and depends on the properties of the dynamic system and command, as well as many other factors, such as experience, effort, and ability. Although no model captures all aspects of human-control behavior, it is often possible to identify control strategies that approximate typical human behavior over a limited period of time [1–3]. Such models can be used to predict closed-loop behavior of HITL systems.

The review paper [4] provides an account of research on modeling human-control behavior. Much of the early human-control literature is based on studies of compensatory behavior, where the human only has access to the error e for feedback instead of both r and y [5–7]. The well-known *crossover model* and *precision model* provide fundamental principles that can be used to predict human compensatory behavior [8–10]. Alternatively, as discussed in [4], there is significantly less work on HITL models for command-following.

It has long been suggested that humans may rely on models for control. The *internal model hypothesis* of neuroscience suggests that the brain constructs models (i.e., internal models) of the dynamic systems with which it interacts, and uses those models to generate control signals [11–17]. Forward and inverse internal models have been proposed [18–28]. Support for the internal model includes evidence of predictive behavior and qualitative comparisons with models [29–40].

More direct evidence of model-based control strategies by humans is provided in [41], which analyzes command-following interactions with linear time invariant (LTI) dynamic sys-

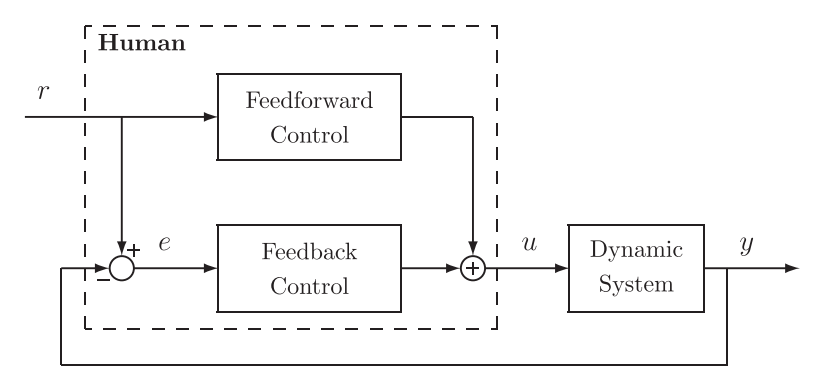


Fig. 1. A control architecture for HITL systems.

Journal of the Franklin Institute xxx (xxxx) xxx

tems. In those studies, the human control response is modeled by the feedback-feedforward control architecture shown in Fig. 1. The feedback control is based on e and models the human's reactive control response; the feedforward control is based only on e and models the human's anticipatory control response. Subsystem identification (SSID) techniques are used to determine best-fit linear models of the feedback and feedforward models. The results in [41] suggest that a primary command-following strategy used by humans is adaptive *feedforward inversion*. Specifically, if the LTI system is represented by the transfer function e, then over repeated interactions the human updates its feedforward controller until it approximates e0-1. SSID results suggest that feedforward inversion is used for many LTI systems, provided that the command is predictable or a preview of the command is available [42,43].

The extent to which humans use adaptive feedforward inversion for control is unknown. Recent results suggest that for some nonminimum-phase LTI systems, the human's feedforward controller does not converge to an approximation of the dynamic system's inverse, but rather a different type of model-based control strategy is used [44]. Thus, it is unclear whether feedforward plant inversion is a primary human-control strategy, even for LTI systems. Human interactions with nonlinear dynamic systems is also an open question. Some studies have investigated HITL interactions with static nonlinear systems and provide some evidence for feedforward inversion [45–51]. However, they do not explicitly identify the controllers used by the human subjects. Moreover, the nonlinear systems used in [45–51] are only static, and thus human control strategies for nonlinear systems having dynamics remains unclear.

The main motivation of this paper is an improved understanding of the command-following control strategies that humans use to interact with nonlinear systems. We present results and analysis of an experiment in which two groups of human subjects interact with two different dynamic systems to perform a command-following task. The first group interacts with a LTI system, and the second group interacts with a Wiener system, which consists of the same LTI dynamics cascaded with a static output nonlinearity. Each subject's command-following behavior is modeled by a discrete-time control architecture consisting of a feedback time delay, a linear feedback controller, and a nonlinear feedforward controller. We compare the time-domain performance and control behavior of these two groups.

This paper provides several new contributions. First, the experimental results suggest that the presence of static output nonlinearities tends to make dynamic systems more difficult for humans to control. Second, we present a new discrete-time nonlinear SSID technique to identify control models that approximate the subjects' command-following behavior. In contrast to existing frequency-domain SSID techniques used in [41,52–55], the SSID technique presented in this paper is performed in the time domain and can accommodate static-input nonlinearities in the feedforward controller. Finally, the identification results are used to address open questions on the impact of dynamic-system nonlinearities on the control strategies that humans use in command-following tasks.

2. Experimental methods and performance data

Twenty-two people voluntarily participated in this study, which was approved by the University of Kentucky's Institutional Review Board under IRB protocol 44649. The subjects were 18 to 35 years old and had no known neurological disorders. Subjects use a rotational joystick (Teledyne Gurley model 8225-6000-DQSD) to control the motion of an object that is displayed on a computer screen. A *trial* is a 60-s time period during which a subject operates the joystick, and a *session* consists of 10 consecutive trials completed within a period of

Journal of the Franklin Institute xxx (xxxx) xxx

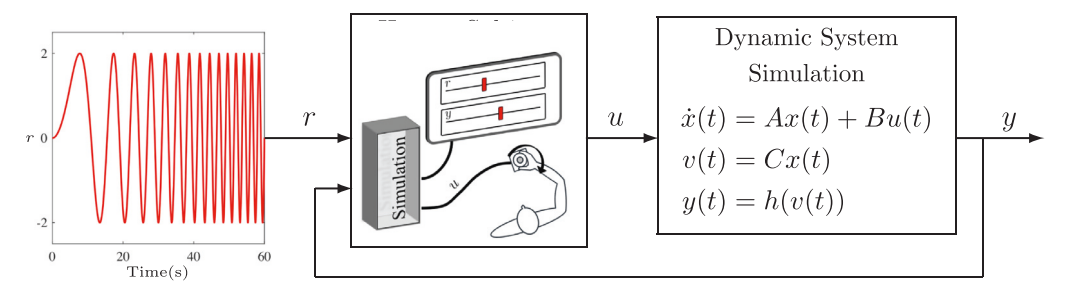


Fig. 2. Subjects use a rotational joystick to control the position y of the bottom marker displayed on the computer screen. The subjects' objective is to make y follow the command r, whose position is displayed on the computer screen by the top marker. The joystick's angular position u is the control input of an unknown dynamic system, which is simulated by a computer, and the dynamic system's output is y.

20 min. Subjects completed 4 sessions over a 7-day period, but no more than one session in a 12-hour period.

The experimental setup is shown in Fig. 2. The computer monitor displays two thin rectangular markers, one above the other. The top rectangular marker is called the *reference object* and its horizontal position is denoted r. The bottom rectangular marker is called the *control object* and its horizontal position is denoted y. The reference object follows a predetermined path, which is the same for all subjects and all trials. Alternatively, the control object's position is dependent on the joystick's angular position, which is denoted by u. The subjects are provided no information about how the joystick affects the motion of the control object. Subjects are instructed to use the joystick to make the control object mimic the motion of the reference object. More specifically, their objective is to generate a control u that makes the magnitude of the command-following error $e \triangleq r - y$ as small as possible.

The reference object's position for all $t \in [0, 60]$ is

$$r(t) \triangleq 2\sin\frac{\pi t^2}{120},\tag{1}$$

which is a 60-second chirp signal with frequency content between 0 and 0.5 Hz. For all $t \in [0, 60]$, the relationship between the subject's control u and the controlled object's position y satisfies the differential equation

$$\dot{x}(t) = Ax(t) + Bu(t),\tag{2}$$

$$v(t) = Cx(t), (3)$$

$$y(t) = h(v(t)), \tag{4}$$

where $x(t) \in \mathbb{R}^n$ is the state, x(0) = 0 is the initial condition, $v(t) \in \mathbb{R}$ is the output of the linear dynamics (which is not accessible to the subjects), $y(t) \in \mathbb{R}$ is the output, $A \in \mathbb{R}^{n \times n}$, $B \in \mathbb{R}^{n \times 1}$, $C \in \mathbb{R}^{1 \times n}$, and $h : \mathbb{R} \to \mathbb{R}$ is a continuous and one-to-one function. It follows from Eqs. (2) and (3) that the transfer function from u to v is $\mathcal{G}(s) \triangleq C(sI - A)^{-1}B$. The units of r and y are hash marks (hm), which are equally-spaced vertical lines displayed on the computer screen. The distance between hash marks is 2.5 cm, and the range of motion displayed on the computer screen is ± 8 hm.

JID: FI [m1+;February 20, 2021;4:13]

S. Koushkbaghi, J.B. Hoagg and T.M. Seigler

Journal of the Franklin Institute xxx (xxxx) xxx

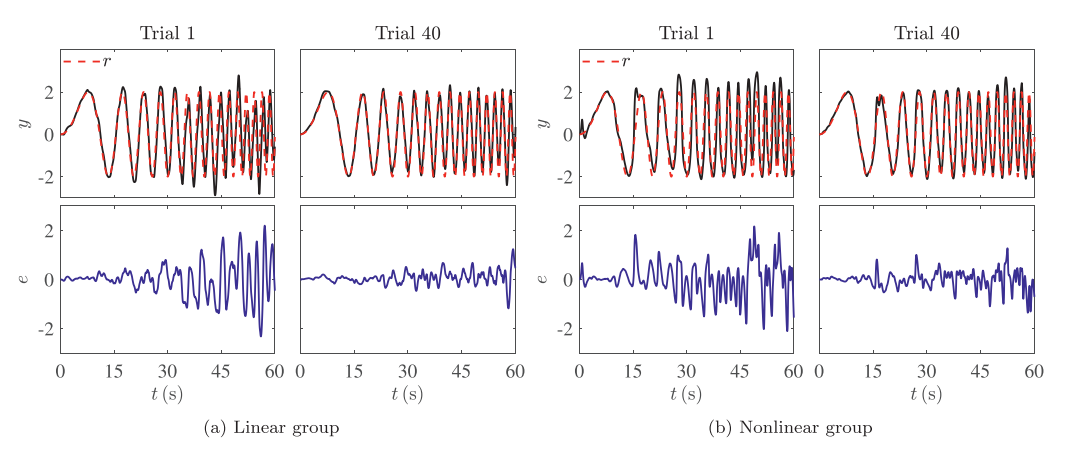


Fig. 3. The reference r_k , output y_k , and error e_k for the median subject's 1st and 40th trial.

The 22 subjects were randomly divided into two groups of 11 subjects. Both groups interacted with the dynamic system (2)–(4), where A, B, and C are the same for both groups. However, h is different for the two groups. The function h is used to explore the effects of nonlinearity on performance and control strategy. For both groups, the transfer function from u to v is

$$\mathcal{G}(s) = \frac{2s + 4.4}{s^2 + 3.6 \ s + 4},$$

which has a zero at -2.2 and a pair of complex-conjugate poles at $-1.8 \pm j0.872$. For the first group, h(v) is the identity function (i.e., h(v) = v), in which case the system (2)–(4) is LTI. We refer to the first group as the *linear group*. For the second group, h(v) is the unique real root of the polynomial $0.1s^3 - 0.2s^2 + 0.5$ s - v. Note that since y = h(v), it follows that

$$h^{-1}(y) = 0.5y - 0.2y^2 + 0.1y^3,$$

which is a cubic nonlinearity. We refer to the second group as the nonlinear group.

For all trials, the experimental time signals r, y, and u are recorded with sample time $T_s = 0.02$ s and $N_s = 3001$ samples. The sampled data yield the discrete signals $\{r_k\}_{k=1}^{N_s}$, $\{y_k\}_{k=1}^{N_s}$, and $\{u_k\}_{k=1}^{N_s}$. The sampled command-following error is $e_k \triangleq r_k - y_k$, and the time-averaged error is

$$||e|| \triangleq \frac{1}{N_{\rm s}} \sum_{k=1}^{N_{\rm s}} |e_k|.$$

A divergent trial is a trial in which the magnitude of y_k exceeds 8 hm, that is, the controlled object's position exceeds the range of motion displayed on the computer screen. There was only one divergent trial in this study, and it is omitted from the results.

Fig. 3 shows r_k , y_k , and e_k on the first and last trial for the median performer in the linear and nonlinear groups. The median performer of each group is the subject whose ||e|| on the last trial is the median (i.e., 6th best) of all subjects in their group. The median subject for both groups performs better on the last trial than the first trial. All subjects in both groups

Journal of the Franklin Institute xxx (xxxx) xxx

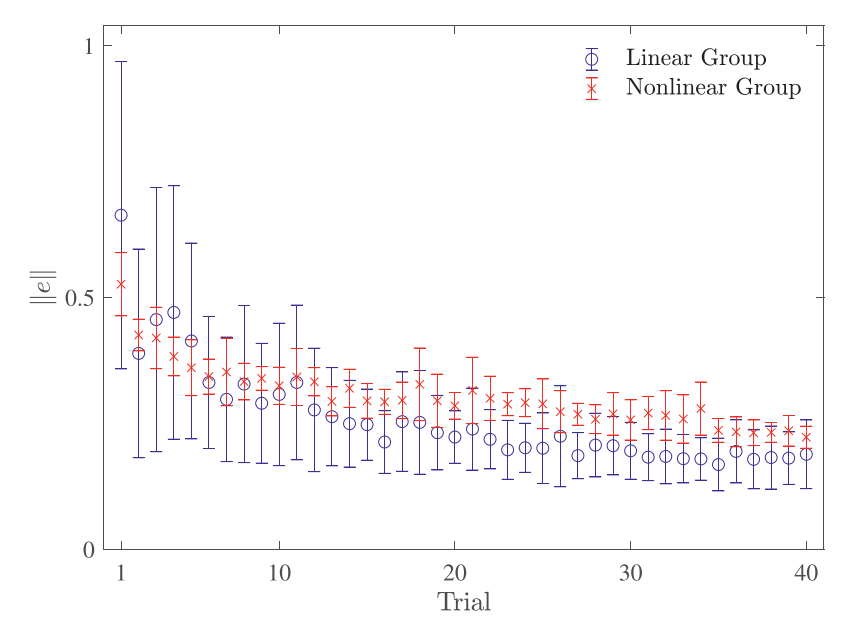


Fig. 4. The performance of both linear and nonlinear groups improves over 40 trials. The symbols \circ and \times indicate the mean of the 11 subjects for linear and nonlinear group respectively and the vertical lines show one standard deviation above and below the mean.

exhibit improved performance from their first to last trial. Similar results are observed for all other subjects.

Fig. 4 shows the mean and standard deviation of ||e|| on each trial. For both the linear and nonlinear group, the mean and standard deviation tend to decrease over the trials. The average ||e|| of the linear group is smaller than the average ||e|| of the nonlinear group on 77.5% of the trials. This suggests that the nonlinear system is more difficult to control than the linear system. However, the linear group exhibits a larger variance in performance on all trials. We note that the variance of the nonlinear group is small compared with the results of several similar experiments [41,44,55]. The reason for this small variance is unclear, but it may be a small-sample effect or possibly caused by some feature of the nonlinearity.

3. Modeling human control behavior

We model each subject's control strategy by the discrete-time control architecture shown in Fig. 5. The dynamic system consists of the pair (G, h), where G(z) is the discrete-time transfer function that is obtained by discretizing $\mathcal{G}(s)$ using a zero-order hold on the input with sample time T_s . The human controller consists of a feedback transfer function $G_{fb}(z)$; a feedback delay d, which is a nonnegative integer (the feedback time delay in seconds is dT_s); feedforward transfer functions $G_{ff,1}(z), \ldots, G_{ff,p}(z)$; and basis functions $f_1, \ldots, f_p : \mathbb{R} \to \mathbb{R}$.

The feedback delay d models physiological limitations associated with visual processing and neuromuscular response. The feedback transfer function $G_{\rm fb}$ models the subjects' reactive control response, which is based on the observed command-following error e_k . The feed-forward transfer functions $G_{{\rm ff},1},\ldots,G_{{\rm ff},p}$ and basis functions f_1,\ldots,f_p model the subjects' anticipatory control response, which is based solely on the command r_k . The basis functions

Journal of the Franklin Institute xxx (xxxx) xxx

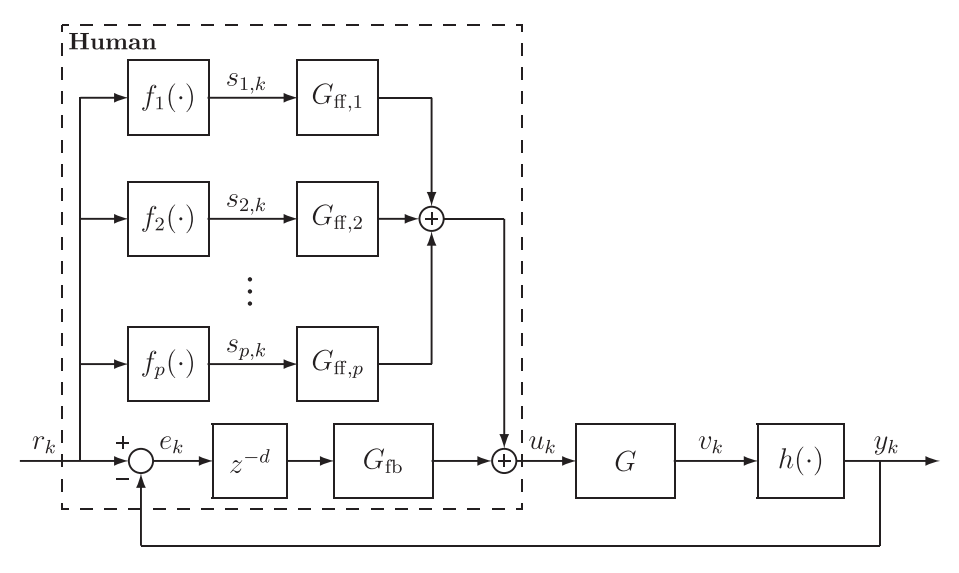


Fig. 5. A time-invariant system, where the input r_k , the output y_k , and the signals v_k and u_k are accessible, but all internal signals are inaccessible.

 f_1, \ldots, f_p allow for static-input nonlinearities in the feedforward controller. Feedforward delay is not included in the control model because the chirp command (1) is predictable and the same for all trials. Physiological interpretations of feedback and feedforward control processes are given in [25].

The SSID problem is to estimate the feedback pair (d, G_{fb}) and feedforward transfer functions $(G_{ff,1},\ldots,G_{ff,p})$ from knowledge of G and h, basis functions f_1,\ldots,f_p , and discrete-time signals r_k and v_k . We note that SSID techniques for modeling HITL systems with LTI systems are given in [54,56–59]. Those techniques are not applicable to the feedback structure of Fig. 5, because of the dynamic-system and controller nonlinearities. To address the nonlinear aspects of this SSID problem, we introduce a new approach that uses concepts from [54] and [60]. Specifically, [60] uses a feedforward architecture similar to Fig. 5 for Hammerstein-model identification, and [54] introduces a convexification approach that involves gridding on the parameters of the feedback pair (d, G_{fb}) .

The following assumptions and notation are used for the rest of this section. Unless otherwise specified, all references to the subscript j are for all $j \in \{1, \ldots, p\}$. Let N and D be the coprime polynomials of degree n_y and d_y satisfying $G = ND^{-1}$. The feedback transfer function $G_{\rm fb}$ has the factorization $G_{\rm fb} = N_{\rm fb}D_{\rm fb}^{-1}$, where $N_{\rm fb}$ are polynomials of degree $n_{\rm fb}$ and $d_{\rm fb}$, where $d_{\rm fb} \geq n_{\rm fb}$. The feedforward transfer function $G_{\rm ff,j}$ is order $n_{\rm ff}$ finite impulse response (FIR), which implies that it can be expressed as $G_{\rm ff,j} = z^{-n_{\rm ff}}N_{\rm ff,j}$, where $N_{\rm ff,j}$ is a polynomial of degree $n_{\rm ff}$. The FIR assumption does not significantly restrict the range of feedforward behavior relative to an infinite impulse response (IIR) transfer function, since a sufficiently large order FIR transfer function can be used to approximate an IIR transfer function to arbitrary accuracy. Next, the discrete signals r_k and v_k have N_s samples and sampling time T_s . Finally, the operator q denotes the forward shift operator (i.e., if x_k is a sequence, then $qx_k = x_{k+1}$).

JID: FI [m1+;February 20, 2021;4:13]

S. Koushkbaghi, J.B. Hoagg and T.M. Seigler

Journal of the Franklin Institute xxx (xxxx) xxx

Let $\hat{v}(z)$ and $\hat{u}(z)$ denote the z-transforms of v_k and u_k , and it follows that:

$$\hat{v}(z) = G(z)\hat{u}(z). \tag{5}$$

The control based on the architecture of Fig. 5 is

$$\hat{u}(z) = G_{\text{fb}}(z)z^{-d}\hat{e}(z) + \sum_{j=1}^{p} G_{\text{ff},j}(z)\hat{s}_{j}(z), \tag{6}$$

where $\hat{e}(z)$ is the z-transform of $e_k = r_k - h(v_k)$, and $\hat{s}_j(z)$ is the z-transforms of $f_j(r_k)$. Combining Eqs. (5) and (6) yields

$$\hat{v}(z) = G(z)G_{\text{fb}}(z)z^{-d}\hat{e}(z) + G(z)\sum_{j=1}^{p} G_{\text{ff},j}(z)\hat{s}_{j}(z). \tag{7}$$

Substituting the polynomials N, D, N_{fb} , D_{fb} , and $N_{\text{ff},j}$ into Eq. (7) and multiplying through by $DD_{\text{fb}}z^{d+n_{\text{ff}}}$ yields

$$D(z)D_{fb}(z)z^{d+n_{ff}}\hat{v}(z) = N(z)N_{fb}(z)z^{n_{ff}}\hat{e}(z) + N(z)D_{fb}(z)z^{d}\sum_{j=1}^{p}N_{ff,j}(z)\hat{s}_{j}(z).$$
(8)

We seek feedback and feedforward parameters that make the left and right side of Eq. (8) approximately equal. Specifically, we seek $N_{\text{ff},1}, \ldots, N_{\text{ff},p}, N_{\text{fb}}, D_{\text{fb}}$, and d that minimize the cost function

$$J(d, N_{\text{fb}}, D_{\text{fb}}, N_{\text{ff},1}, \dots, N_{\text{ff},p}) \triangleq \frac{1}{2} \sum_{k=1-\ell_d}^{N_{\text{s}}-\ell_d} |N(\mathbf{q})D_{\text{fb}}(\mathbf{q})\mathbf{q}^d \sum_{j=1}^p N_{\text{ff},j}(\mathbf{q})f_j(r_k) + N(\mathbf{q})N_{\text{fb}}(\mathbf{q})\mathbf{q}^{n_{\text{ff}}}e_k - D(\mathbf{q})D_{\text{fb}}(\mathbf{q})\mathbf{q}^{d+n_{\text{ff}}}v_k|^2,$$

where $\ell_d \triangleq d + n_{\rm ff} + d_y + d_{\rm fb}$. To identify $N_{\rm ff,j}$, $N_{\rm fb}$, $D_{\rm fb}$, and d, we first generate a *candidate pool* that contains $N_{\rm c}$ possible models of the feedback pair $(d, G_{\rm fb})$. The cost J is convex in the coefficients of $N_{\rm ff,j}$. For each feedback pair $(d, G_{\rm fb})$ in the candidate pool, a convex optimization is solved to determine the best-fit $N_{\rm ff,j}$ that minimizes $J(N_{\rm ff,j})$. This computation generates $N_{\rm c}$ models of $(d, N_{\rm fb}, D_{\rm fb}, N_{\rm ff,j})$, from which we select the element that minimizes $J(d, N_{\rm fb}, D_{\rm fb}, N_{\rm ff,j})$. A detailed description of the SSID algorithm is given in Appendix A. Properties of this SSID algorithm can be derived using analyses similar to those given in [54], which shows that if the data noise is sufficiently small and the feedback candidate pool is sufficiently dense, then the identified control parameters are arbitrarily close to the true parameters. Appendix C provides numerical examples that demonstrate the application and effectiveness of this SSID method.

4. Potential human control strategies

We consider control strategies that are possible solutions of the SSID algorithm of Section 3. The focus of this section is on control strategies for the nonlinear group. For the rest of this section, we assume that the pair (G, h) in Fig. 5 is that of the nonlinear group. For the linear group, there is a wide range of linear-control strategies that can be used to achieve closed-loop stability and good command-following performance. Some of these linear-control strategies and their limitations for HITL applications are discussed in [41].

Journal of the Franklin Institute xxx (xxxx) xxx

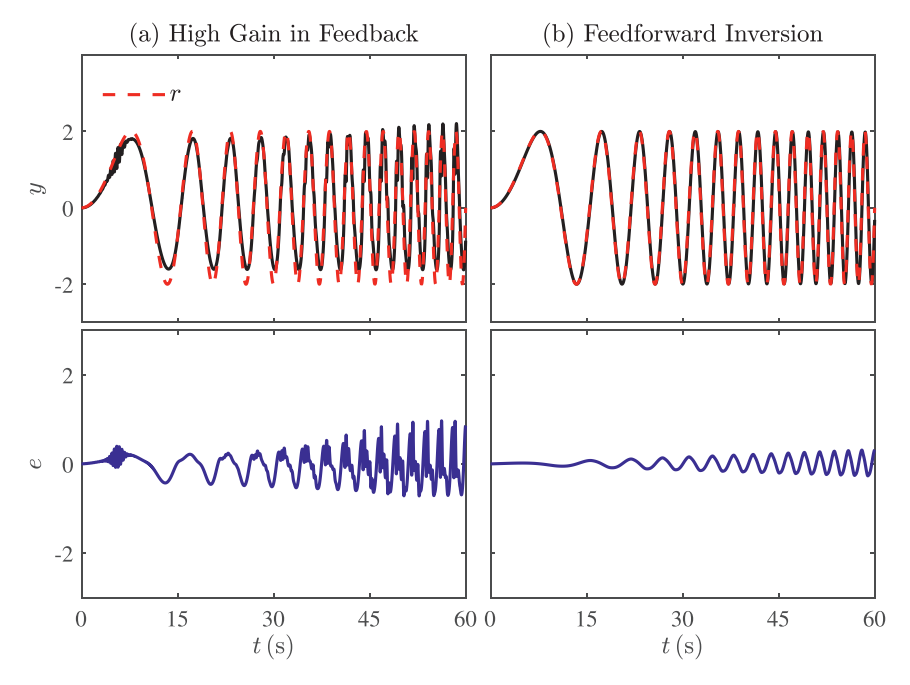


Fig. 6. Two different control strategies that make the magnitude of the error small for the nonlinear group: (a) High gain in feedback; (b) Approximate inverse dynamics in feedforward.

First, consider a pure feedback control strategy. For all $j \in \{1, ..., p\}$, let $G_{\mathrm{ff}, j} = 0$. In this case, the control architecture of Fig. 5 reduces to a Lur'e system. One possible control strategy is high gain in feedback, which makes the Bode magnitude large at frequencies of the command r_k . High-gain in feedback yields good command-following performance for LTI systems, provided that the closed-loop is asymptotically stable. Closed-loop stability and performance for the nonlinear system (G,h) is more difficult to evaluate. Since the slope of the magnitude of h is bounded, there are several classical nonlinear stability results that apply [61]. For example, the circle criterion implies that the closed-loop system is absolutely stable if $G_{\mathrm{fb}}G$ is asymptotically stable and its H_{∞} norm is sufficiently small [61, Theorem 5.2].

Consider the feedback transfer function $G_{\rm fb} = 6.67z/(z^2 - 0.07z + 0.8)$. Let the feedback delay be d = 5, which corresponds to a feedback time delay of 100 ms. Fig. 6 shows the resulting closed-loop output y_k and error e_k . The time-averaged error corresponding to Fig. 6 is 0.24, which is smaller than time-averaged error for all 40th trial experiments of the nonlinear group (cf. Fig. 4).

There are some practical limitations for using high-gain in feedback for manual command-following tasks. Humans cannot use arbitrarily high gain due to physical limitations in speed and range of motion. Moreover, a human's ability to use high gain in feedback is limited by their feedback time delay, which can cause closed-loop instability if the gain in feedback is too large.

Another possible control strategy is feedforward inversion. Let p = 3, $f_1(r_k) = 0.5r_k$, $f_2(r_k) = -0.2r_k^2$, $f_3(r_k) = 0.1r_k^3$, and $G_{\text{ff},j} = G^{-1}$ for all $j \in \{1, 2, 3\}$. If in addition $G_{\text{fb}} = 0$, then the closed-loop response is $\hat{e} = [1 - G^{-1}G]\hat{r} = 0$, which implies that the command-following error is zero. Similar performance results can also be obtained by approximate feed-

Journal of the Franklin Institute xxx (xxxx) xxx

forward inversion, where the feedforward controllers are approximations of G^{-1} . Fig. 6 shows the resulting closed-loop output y_k and error e_k for the case that for all $j \in \{1, 2, 3\}$, $G_{\text{ff}, j}$ is the matched z-transform mapping of $22 G^{-1}(s)/(s+22)$, which is a proper approximation of G^{-1} . We note that the approximate feedforward inversion controller yields a better performance than the median-performer's 40th-trial results shown in Fig. 3. The time-averaged error corresponding to Fig. 6 is 0.09, which is smaller than time-averaged error for all 40th trial experiments of the nonlinear group (cf. Fig. 4).

As with high gain in feedback, there may also be practical limitations with feedforward inversion. In particular, a human's ability to approximate the dynamic-system inverse may be limited by various features, such as relative degree, time delays, and nonminimum-phase zeros [55]. Nonlinearities may also inhibit accurate approximation of the dynamic-system inverse.

There are many other control strategies of the form (6) that yield good command-following performance. Another possible strategy is a combination of high gain in feedback and feedforward inversion. For example, humans may use high-gain feedback at lower frequencies, where they have more control authority and the effects of feedback time delay are less pronounced; and then at higher frequencies, humans may utilize their predictive capabilities to implement feedforward inversion to mitigate the effects of reduced control authority and increased phase lag due to time delay.

5. Results and discussion

The SSID method described in Section 3 is applied to the experimental data of the linear and nonlinear groups. For each subject and each trial, we identify a feedback transfer function $G_{\rm fb}$, feedback delay d, and feedforward transfer functions $G_{\rm ff,1},\ldots,G_{\rm ff,p}$. The candidate pool Γ contains approximately 50 million candidate pairs $(d,G_{\rm fb})$ and captures a wide range control behavior over the 0-to-0.5 Hz frequency range of the command (1). The candidate feedback transfer functions $G_{\rm fb}$ are second order relative degree one with monic denominator (i.e., $n_{\rm fb}=1$, and $d_{\rm fb}=2$). More specific details on the candidate pool are provided in Appendix B. The feedforward transfer functions $G_{\rm ff,1},\ldots,G_{\rm ff,p}$ are each 5th-order FIR, and for $i\in\{1,\ldots,5\}$, $f_i(r_k)=r_k^i$. The SSID algorithm is implemented using parallel computation on a supercomputer. A validation analysis of the identification results is presented in Appendix D.

We first present identification results of the feedback pair (d, G_{fb}) . For each identified feedback transfer function, we define

$$\|G_{\mathrm{fb}}\| \triangleq \max_{\omega \in [0,\pi]} \left| G_{\mathrm{fb}}(e^{l\omega T_{\mathrm{s}}}) \right|,$$

which is the peak magnitude of the feedback transfer function over the 0-to-0.5 Hz range of the command r. For each trial, we compute the average $\|G_{\rm fb}\|$ and average time delay d of all 11 subjects in each group. Figs. 7 and 8 show the trial-by-trial averages for the linear and nonlinear groups. The subjects in the nonlinear group consistently use a lower feedback gain and a larger time delay than the subjects in the linear group. The larger time delay suggests that the nonlinear-group subjects are more hesitant to react to command-following errors than the linear-group subjects. The larger time delay for the nonlinear subjects limits the amount of gain they can use in feedback to maintain a stable closed-loop response. In contrast, the linear-group subjects have a smaller time delay and are thus able to use larger feedback gain.

Next, identification results are presented for the feedforward controllers. For all $k \in \{1, ..., N_s\}$, define the identified feedforward control signal $u_{ff,k} \triangleq \sum_{j=1}^{p} N_{ff,j}(q) f_j(r_k)$. We

Journal of the Franklin Institute xxx (xxxx) xxx

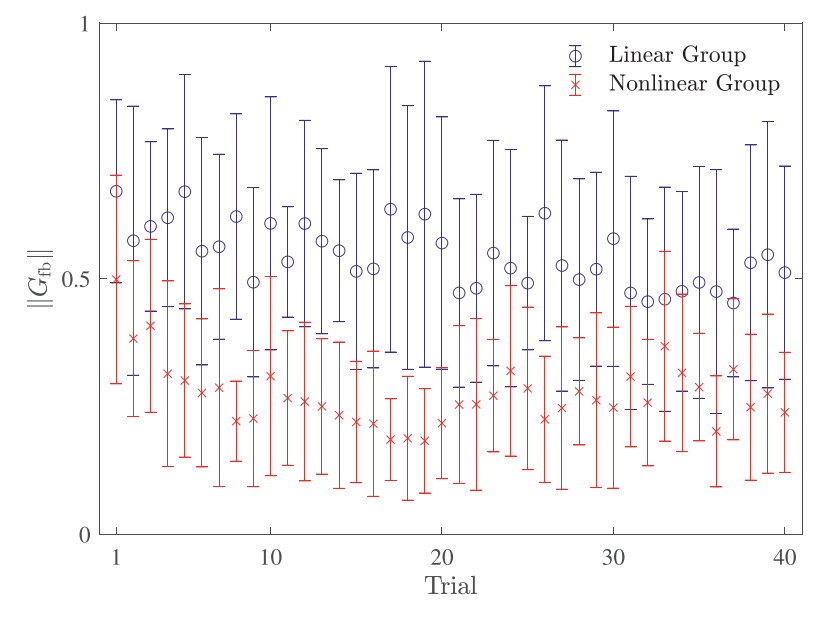


Fig. 7. The feedback controller's peak magnitude for the nonlinear group is smaller than that of the linear group over all 40 trials. The symbols \circ and \times indicate the mean of the 11 subjects for linear and nonlinear group respectively and the vertical lines show one standard deviation above and below the mean.

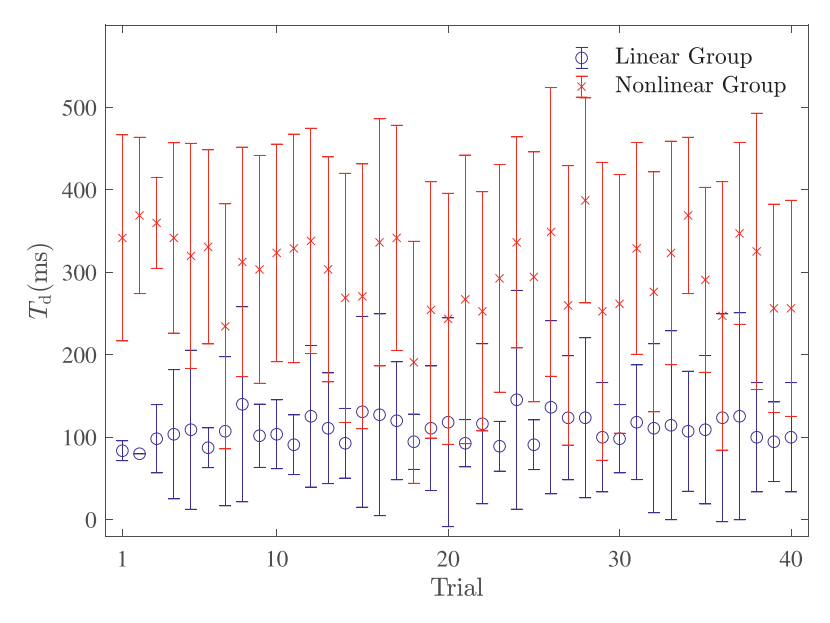


Fig. 8. Subjects in the nonlinear group have more feedback delay over the 40 trials compared to subjects in the linear group. The symbols \circ and \times indicate the mean of the 11 subjects for linear and nonlinear group respectively and the vertical lines show one standard deviation above and below the mean.

JID: FI

Journal of the Franklin Institute xxx (xxxx) xxx

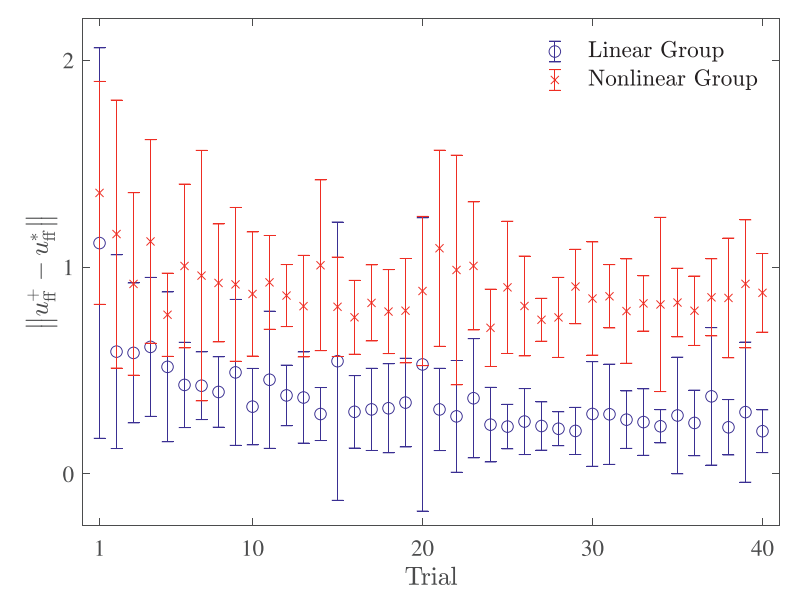


Fig. 9. The time-averaged difference between $u_{\mathrm{ff},k}$ and $u_{\mathrm{ff},k}^*$ for the linear and nonlinear group decreases over 40 trials. The symbols \circ and \times indicate the mean of the 11 subjects for linear and nonlinear group respectively and the vertical lines show one standard deviation above and below the mean.

compare $u_{\mathrm{ff},k}$ with the feedforward-inversion control signal $u_{\mathrm{ff},k}^*$, which is the zero-initial-condition solution of $u_{\mathrm{ff},k}^* \triangleq G^{-1}(q)h^{-1}(r_k)$. For each identified feedback controller, the average difference between $u_{\mathrm{ff},k}$ and $u_{\mathrm{ff},k}^*$ is defined as

$$||u_{\rm ff} - u_{\rm ff}^*|| \triangleq \frac{1}{N_{\rm s}} \sum_{k=1}^{N_{\rm s}} |u_{{\rm ff},k} - u_{{\rm ff},k}^*|.$$

A smaller $\|u_{\rm ff} - u_{\rm ff}^*\|$ indicates that the feedforward controller more closely approximates feedforward inversion. Fig. 9 shows the average $\|u_{\rm ff} - u_{\rm ff}^*\|$ of the 11 subjects in the linear and nonlinear groups for each trial. For both groups, the average of $\|u_{\rm ff} - u_{\rm ff}^*\|$ decreases over the 40 trials. The linear group's feedforward control is on average a better approximation of feedforward inversion than the nonlinear group. This difference may account for some of the difference in performance between the two groups (see Fig. 4). Specifically, the dynamic system's static output nonlinearity may make it more difficult for the subjects to accurately invert the dynamics in feedforward, thus yielding decreased performance.

The results in Fig. 9 suggest that both groups of subjects learn to approximate the dynamic system's inverse in feedforward. To distinguish between the learning of G^{-1} and h^{-1} for the nonlinear group, we use each subject's identified controller to derive a Hammerstein-model approximation of their feedforward controller. Specifically, we compute a pair $(f, G_{\rm ff})$ where $f: \mathbb{R} \to \mathbb{R}$ is an input nonlinearity, $G_{\rm ff}$ is a FIR transfer function, and $G_{\rm ff}(q)f(r_k)$ is the Hammerstein-model approximation. Note that the identified feedforward control $\sum_{j=1}^p G_{\rm ff,j}(q)f_j(r_k)$ is a Hammerstein model if for all $j \in \{1, \ldots, p\}$, there exists scalar c_j such that $G_{\rm ff,j} = c_j G_{\rm ff}$. The Hammerstein model structure is more restrictive feedforward control model than that of Fig. 5. However, when the feedforward controller

Journal of the Franklin Institute xxx (xxxx) xxx

approximates feedforward inversion, then a Hammerstein model pair $(f, G_{\rm ff})$ can approximate this behavior and provide a direct comparison with the components of the exact feedfoward inversion pair (h^{-1}, G^{-1}) .

Replacing the feedforward controller in (8) with the Hammerstein model $(f, G_{\rm ff})$ yields

$$D(z)D_{\text{fb}}(z)z^{d+n_{\text{ff}}}\hat{v}(z) = N(z)N_{\text{fb}}(z)z^{n_{\text{ff}}}\hat{e}(z) + N(z)D_{\text{fb}}(z)z^{d}G_{\text{ff}}(z)\hat{s}(z), \tag{9}$$

where $\hat{s}(z)$ is the z-transform of $f(r_k)$. Let f be defined by $f(r_k) \triangleq \sum_{j=1}^p \alpha_j f_j(r_k)$, where $\alpha_1, \ldots, \alpha_p \in \mathbb{R}$ are unknown coefficients. We assume that the linear behavior of the identified feedforward controller is primarily captured by its linear component $G_{\mathrm{ff},1}(q)f_1(r_k)$, and we let $G_{\mathrm{ff}} = \frac{1}{\alpha_1}G_{\mathrm{ff},1}$. Thus, the Hammerstein model can be expressed as $G_{\mathrm{ff}}(q)f(r_k) = G_{\mathrm{ff},1}(q)\bar{f}(r_k)$, where

$$\bar{f}(r_k) \triangleq f_1(r_k) + [f_2(r_k) \quad \cdots \quad f_p(r_k)]\bar{\alpha},$$

and $\bar{\alpha} \triangleq \left[\frac{\alpha_2}{\alpha_1} \cdots \frac{\alpha_p}{\alpha_1}\right]^T$. We use (9) along with the identified control components d, $G_{\rm fb}$, and $G_{\rm ff,1}$ to find a best-fit $\bar{\alpha}$. For all $k \in \{1 - \ell_d, \dots, N_{\rm S} - \ell_d\}$, define

$$m_k \triangleq N(q)D_{fb}(q)N_{ff,1}(q)q^d[f_2(r_k) \cdots f_p(r_k)],$$

 $n_k \triangleq D(q)D_{fb}(q)q^{d+n_{ff}}v_k - N(q)N_{fb}(q)q^{n_{ff}}e_k - N(q)D_{fb}(q)N_{ff,1}(q)q^df_1(r_k),$

where d, $N_{\rm fb}$, $D_{\rm fb}$, and $N_{\rm ff,1}$ are identified parameters. For all $k=1,\ldots,N_{\rm f}$, let $\omega_k\triangleq (k-1)\pi/30$ rad/s, which are $N_{\rm f}=31$ evenly-spaced frequencies over the 0-0.5 Hz range. Let $m_{\rm dft}(\omega_k)$ and $n_{\rm dft}(\omega_k)$ denote the discrete Fourier transforms of the sequences $\{m_{k-\ell_d}\}_{k=1}^{N_{\rm s}}$ and $\{n_{k-\ell_d}\}_{k=1}^{N_{\rm s}}$. We seek $\bar{\alpha}$ that minimizes the cost function

$$\mathcal{J}_{\mathrm{H}}(\bar{\alpha}) \triangleq \sum_{\omega_k \in [\omega_1, \omega_{N_k}]} |m_{\mathrm{dft}}(\omega_k)\bar{\alpha} - n_{\mathrm{dft}}(\omega_k)|^2.$$

The cost \mathcal{J}_H is convex in the elements of $\bar{\alpha}$. The method of least squares is used to determine the best-fit $\bar{\alpha}$ that minimizes \mathcal{J}_H .

The Hammerstein-model pair is $(\alpha_1 \bar{f}, G_{\mathrm{ff},1}/\alpha_1)$, where α_1 is unknown. Note that for any nonzero α_1 , $\frac{1}{\alpha_1}G_{\mathrm{ff},1}(q)\alpha_1 \bar{f}(r_k) = G_{\mathrm{ff},1}(q)\bar{f}(r_k)$. Thus, α_1 is an arbitrary with regards to the input-output response. To compare (f, G_{ff}) with (h^{-1}, G^{-1}) , we let

$$\alpha_{1} \triangleq \frac{\sqrt{\sum_{k=1}^{N_{s}} \left| h^{-1}(r_{k}) \right|^{2}}}{\sqrt{\sum_{k=1}^{N_{s}} \left| \bar{f}(r_{k}) \right|^{2}}},\tag{10}$$

which enforces the condition that $\{f(r_k)\}_{k=1}^{N_s}$ and $\{h^{-1}(r_k)\}_{k=1}^{N_s}$ have the same ℓ_2 norm.

For each subject and each trial, we identify a best-fit Hammerstein model pair $(f, G_{\rm ff})$. The following discussion compares the subjects' identified feedforward components f and $G_{\rm ff}$ with the ideal feedforward inversion components h^{-1} and G^{-1} .

First, we compare f with h^{-1} . Fig. 10 shows the average f for all subjects on the first and last trials of the linear and nonlinear groups. For both groups, the average f is a better approximation of h^{-1} on the last trial than on the first trial. The nonlinear group has a more significant change in f from the first to the last trial. To further compare f with h^{-1} , define

$$||f - h^{-1}|| \triangleq \frac{1}{2} \sum_{k=1}^{N_s} \frac{|f(r_k) - h^{-1}(r_k)|}{|h^{-1}(r_k)|},$$

JID: FI [m1+;February 20, 2021;4:13]

S. Koushkbaghi, J.B. Hoagg and T.M. Seigler

Journal of the Franklin Institute xxx (xxxx) xxx

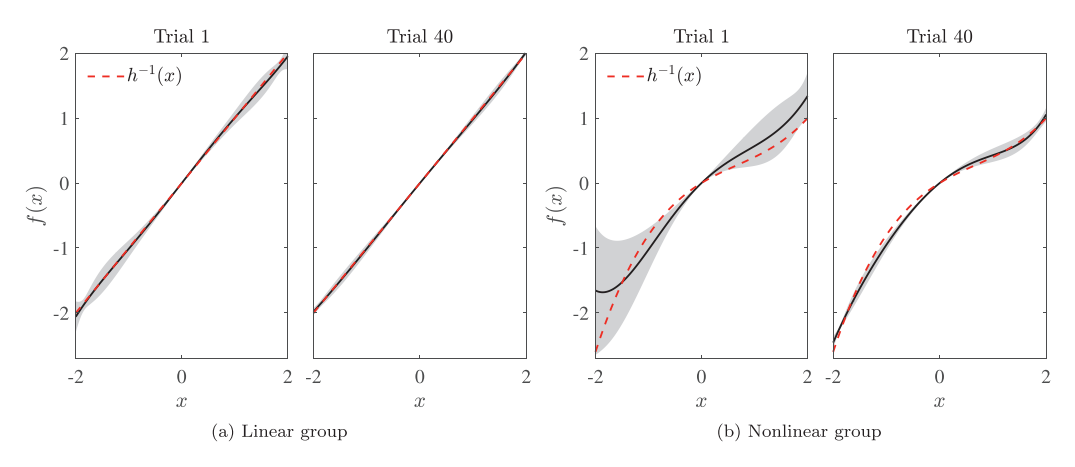


Fig. 10. The average basis function f is a better approximation of h on the last trial than the first trial. The shaded region shows one standard deviation above and below the mean.

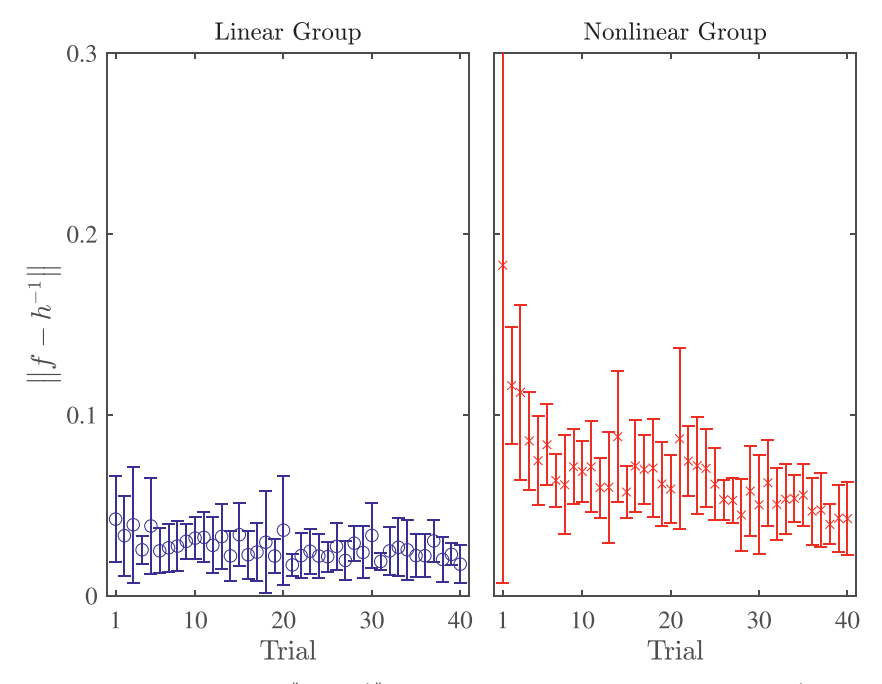


Fig. 11. Mean and standard deviation of $||f - h^{-1}||$ on each trial. The difference between f and h^{-1} for the nonlinear group has a more significant decreases over the 40 trials. The symbols \circ and \times indicate the mean of 11 subjects for the linear and nonlinear group respectively and the vertical lines show one standard deviation above and below the mean.

which is a measure of the difference between f and h^{-1} . Fig. 11 shows the mean and standard deviation of $||f - h^{-1}||$ on each trial of the linear and nonlinear group. The average of $||f - h^{-1}||$ is smaller for the linear group than the nonlinear group on all trials. For both groups, the average of $||f - h^{-1}||$ is smaller on the last trial compared to the first trial. However, the nonlinear group exhibits a more significant decreasing trend over the 40 trials.

JID: FI

Journal of the Franklin Institute xxx (xxxx) xxx

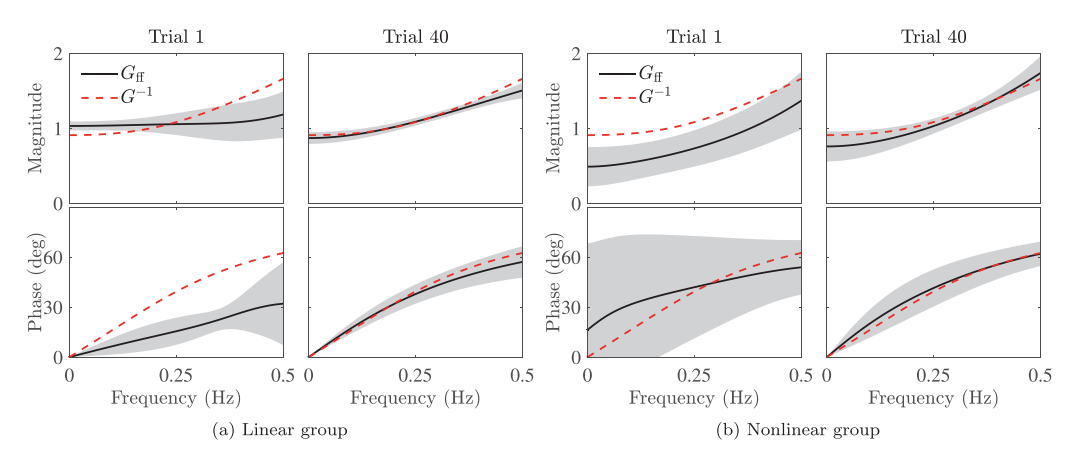


Fig. 12. The average feedforward transfer function $G_{\rm ff}$ approximates G after 40 trials. The shaded region shows one standard deviation above and below the average identified feedforward transfer function.

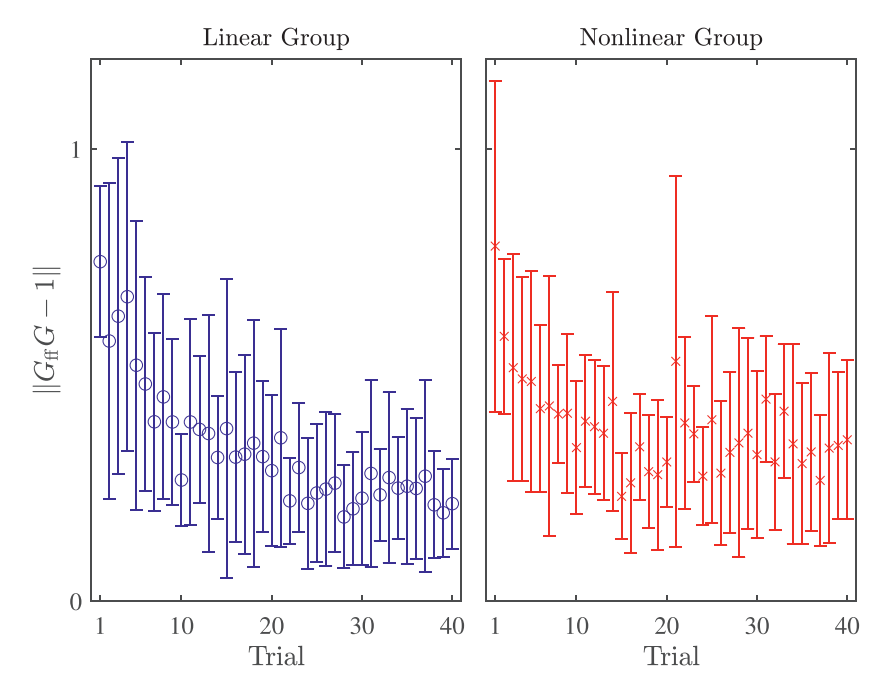


Fig. 13. Mean and standard deviation of $\|G_{\rm ff}G - 1\|$ on each trial. For both groups, the difference between $G_{\rm ff}$ and G^{-1} decreases over the 40 trials. The symbols \circ and \times indicate the mean of the 11 subjects for linear and nonlinear group respectively and the vertical lines show one standard deviation above and below the mean.

These results suggest that the nonlinear subjects learn to approximate h^{-1} in feedforward, whereas there is less learning for the linear group. We also note that the average of $||f - h^{-1}||$ for the nonlinear group continues to decrease over the last 10 trials, suggesting that the subjects may continue to improve their approximation of h^{-1} if given more trials.

Next, we compare $G_{\rm ff}$ with G^{-1} . Fig. 12 shows the average Bode plot over the frequency range of 0-to-0.5 Hz of the identified $G_{\rm ff}$ for all 11 subjects on the first and last trials of the

Journal of the Franklin Institute xxx (xxxx) xxx

linear and nonlinear group. For both groups, the average feedforward transfer function more closely approximates G^{-1} on the last trial compared to the first trial. To further compare $G_{\rm ff}$ with G^{-1} , define

$$\|G_{\mathrm{ff}}G - 1\| \stackrel{\Delta}{=} \frac{1}{\pi} \int_0^{\pi} \left| G_{\mathrm{ff}}(e^{j\omega T_{\mathrm{s}}}) G(e^{j\omega T_{\mathrm{s}}}) - 1 \right| \mathrm{d}\omega,$$

which is a frequency-domain measure of the difference between $G_{\rm ff}$ and G^{-1} . Fig. 13 shows the mean and standard deviation of $\|G_{\rm ff}G - 1\|$ for each trial of the linear and nonlinear group. We note that the trends for the linear group are comparable to those in [44], which applies a frequency-domain SSID method to the same experimental data.

The average of $||G_{\rm ff}G - 1||$ for the two groups have a similar trend over the 40 trials. Over the first 10 trials, there is a decreasing trend for both groups; and over the last 10 trials, the trend is relatively flat for both groups. The linear group achieves a better approximation of G^{-1} than the nonlinear group. These results suggest that the subjects of both groups learn to approximate the inverse of G in feedforward over the 40 trials.

6. Summary and conclusions

This paper presents new results on the impact of nonlinearities on HITL control behavior. The experimental results indicate that static output nonlinearities can make a dynamic system more difficult for humans to control. The average command-following performance of the linear group is better on 77.5% of trials than the nonlinear group (see Fig. 4). To investigate the control strategies of both groups, a nonlinear SSID algorithm is used to identify best-fit feedback and feedforward controllers for each subject and on each trial. The SSID results reveal several differences between the linear and nonlinear groups. The linear group tends to use more feedback-control authority. Specifically, the linear group has a smaller feedback time delay and uses a larger feedback gain than the nonlinear group (see Figs. 7 and 8).

The main finding of this paper addresses feedforward behavior. Prior HITL studies suggest that adaptive feedforward inversion is a primary command-following control strategy for many linear systems. The results in this paper provide supporting evidence that humans also adopt this control strategy for some nonlinear systems. For both the linear and nonlinear groups, the identified feedforward controllers approximate the dynamic system's inverse better on the last trial than on the first trial (see Figs. 10 and 12). However, the linear group achieves better approximation of the dynamic system's inverse (see Figs. 11 and 13). This difference in approximating the inverse is a possible explanation for the difference in performance between the two groups. Finally, the SSID results suggest that the nonlinear subjects learn the linear part of the dynamic system more quickly than they learn the static output nonlinearity. Over the latter half of the trials, the nonlinear subjects' feedforward transfer function does not change significantly (see Fig. 13), whereas they continue to learn the output nonlinearity (see Fig. 11). Given more trials, the nonlinear subjects may continue to learn a better approximation of the dynamic system's inverse and perform as well as the linear subjects.

The results from this study provide some insight into human-control strategies for non-linear systems. However, many open questions remain. Further investigation is needed into whether these results extend to dynamic systems with more complex transfer functions (e.g., higher order, higher relative degree, nonminimum phase, etc.) and more complex output non-linearities. The control strategies that humans use for systems with dynamic nonlinearities is also a significant open question.

[m1+;February 20, 2021;4:13]

Declaration of Competing Interest

The authors declare that they have no known competing financial interests or personal relationships that could have appeared to influence the work reported in this paper.

Appendix A. SSID Algorithm

To formulate the SSID algorithm in terms of coefficients of the feedback and feedforward controllers, define the candidate polynomials

$$\begin{split} \mathcal{N}_{\text{fb}}(\mathbf{q},\theta) &\triangleq [\mathbf{q}^{n_{\text{fb}}} \quad \mathbf{q}^{n_{\text{fb}}-1} \quad \cdots \quad 1 \quad \mathbf{0}_{1 \times d_{\text{fb}}}]\theta, \\ \mathcal{D}_{\text{fb}}(\mathbf{q},\theta) &\triangleq \mathbf{q}^{d_{\text{fb}}} + [\mathbf{0}_{1 \times (n_{\text{fb}}+1)} \quad \mathbf{q}^{d_{\text{fb}-1}} \quad \cdots \quad 1]\theta, \\ \mathcal{N}_{\text{ff.},i}(\mathbf{q},\phi_i) &\triangleq [\mathbf{q}^{n_{\text{ff}}} \quad \mathbf{q}^{n_{\text{ff}}-1} \quad \cdots \quad 1]\phi_i, \end{split}$$

where $\theta \in \mathbb{R}^{n_{\text{fb}}+d_{\text{fb}}+1}$ contains the numerator and denominator coefficients of feedback transfer function, and $\phi_j \in \mathbb{R}^{n_{\text{ff}}+1}$ contains the numerator coefficients of the feedforward transfer function. Next, consider the cost function

$$\mathcal{J}(\delta,\theta,\phi) \triangleq J(\delta,\mathcal{N}_{\mathrm{fb}}(\mathbf{q},\theta),\mathcal{D}_{\mathrm{fb}}(\mathbf{q},\theta),\mathcal{N}_{\mathrm{ff},j}(\mathbf{q},\phi_j)) = \frac{1}{2} \sum_{k=1-\ell_{\delta}}^{N_{\mathrm{s}}-\ell_{\delta}} |a_k(\delta,\theta)\phi - b_k(\delta,\theta)|^2,$$

where the positive integer δ is the feedback delay, $\ell_{\delta} \triangleq \delta + n_{\rm ff} + d_{\rm y} + d_{\rm fb}$, $\phi \triangleq [\phi_1^{\rm T} \cdots \phi_n^{\rm T}]^{\rm T} \in \mathbb{R}^{p(n_{\rm ff}+1)}$, and for all $k \in \{1 - \ell_{\delta}, \dots, N_{\rm s} - \ell_{\delta}\}$,

$$a_k(\delta,\theta) \triangleq N(\mathbf{q})\mathcal{D}_{\mathrm{fb}}(\mathbf{q},\theta)\mathbf{q}^{\delta}[\mathbf{q}^{n_{\mathrm{ff}}} \quad \mathbf{q}^{n_{\mathrm{ff}}-1} \quad \cdots \quad 1] \otimes [f_1(r_k) \quad \cdots \quad f_p(r_k)] \in \mathbb{R}^{1 \times p(n_{\mathrm{ff}}+1)},$$

$$b_k(\delta,\theta) \triangleq D(\mathbf{q})\mathcal{D}_{\mathrm{fb}}(\mathbf{q},\theta)\mathbf{q}^{\delta+n_{\mathrm{ff}}}v_k - N(\mathbf{q})\mathcal{N}_{\mathrm{fb}}(\mathbf{q},\theta)\mathbf{q}^{n_{\mathrm{ff}}}e_k \in \mathbb{R},$$

where \otimes denotes the Kronecker product.

Next, let $\mathcal{I}_c \triangleq \{1, \dots, N_c\}$, where N_c is a positive integer. For all $i \in \mathcal{I}_c$, define distinct candidate feedback pairs (δ_i, θ_i) . Let Γ be a set with N_c elements where $\gamma_i \triangleq \begin{bmatrix} \delta_i & \theta_i^T \end{bmatrix}^T \in \mathbb{R}^{n_{\text{fb}} + d_{\text{fb}} + 2}$ are its elements. We call Γ the *candidate pool*. For each $\gamma_i \in \Gamma$, define the quadratic cost function

$$\mathcal{J}_i(\phi) \triangleq \frac{1}{2} \|A_i \phi - b_i\|_2^2,$$

where

$$A_i \triangleq [a_{1-\ell_{\delta_i}}^{\mathsf{T}}(\delta_i, \theta_i) \quad a_{2-\ell_{\delta_i}}^{\mathsf{T}}(\delta_i, \theta_i) \quad \cdots \quad a_{N_s-\ell_{\delta_i}}^{\mathsf{T}}(\delta_i, \theta_i)]^{\mathsf{T}} \in \mathbb{R}^{N_s \times p(n_{\mathrm{ff}}+1)},$$

$$b_i \triangleq [b_{1-\ell_{\delta_i}}(\delta_i, \theta_i) \quad b_{2-\ell_{\delta_i}}(\delta_i, \theta_i) \quad \cdots \quad b_{N_s-\ell_{\delta_i}}(\delta_i, \theta_i)]^{\mathsf{T}} \in \mathbb{R}^{N_s}.$$

For all $i \in \mathcal{I}_c$, \mathcal{J}_i is quadratic with respect to the unknown feedforward parameters ϕ . If the number of samples N_s is sufficiently large, then it can be shown that $A_i^T A_i$ is positive definite. For each $i \in \mathcal{I}_c$, define

$$\phi_i \triangleq (A_i^{\mathrm{T}} A_i)^{-1} A_i^{\mathrm{T}} b_i,$$

which is the unique global minimizer of \mathcal{J}_i .

Let $\kappa \in \mathcal{I}_c$ be the smallest integer such that $\mathcal{J}_{\kappa} = \min_{i \in \mathcal{I}_c} \mathcal{J}_i$. The identified feedback time delay is $d \triangleq \delta_{\kappa}$; the numerator and denominator polynomials of the identified feedback transfer function are $N_{\text{fb}}(z) \triangleq \mathcal{N}_{\text{fb}}(z, \theta_{\kappa})$ and $D_{\text{fb}}(z) \triangleq \mathcal{D}_{\text{fb}}(z, \theta_{\kappa})$; and the identified feedforward transfer functions are $G_{\text{ff},j}(z) \triangleq z^{-n_{\text{ff}}} \mathcal{N}_{\text{ff},j}(z, \phi_{j,\kappa})$.

Journal of the Franklin Institute xxx (xxxx) xxx

Appendix B. Candidate Pool

The candidate pool Γ is a set that contains approximately 50 million elements and is designed to capture a wide range of possible human control behavior over the 0-to-0.5 Hz frequency range. Candidate feedback transfer functions are second-order IIR with monic denominator and relative degree one, that is, $n_{\rm fb} = 1$, and $d_{\rm fb} = 2$. For each $\gamma \in \Gamma$, the following conditions hold:

- C1) If $\lambda \in \mathbb{C}$ is a root of the candidate polynomial \mathcal{N}_{fb} , then $|\lambda| < 1$.
- C2) If $\lambda \in \mathbb{C}$ is a root of the candidate polynomial \mathcal{D}_{fb} , then $|\lambda| < 1$.

C3)
$$\max_{\omega \in [0,\pi]} \left| \frac{\mathcal{N}_{\text{fb}}(e^{j\omega T_s})}{\mathcal{D}_{\text{fb}}(e^{j\omega T_s})} \right| \leq 30.5.$$

C4)
$$\delta \in \{4, 5, 6, \dots, 25\}.$$

Conditions C1 and C2 indicate that the parameters of candidate feedback controller are designed such that the zero and poles of G_{fb} lie inside the unit circle. Thus, the candidate pool assumes that the feedback control behavior of the subjects is stable. Condition C3 states that the peak magnitude of the feedback controller over the frequency range $[0, \pi]$ rad/s is no more than 30.5 (or approximately 30 dB). Thus, C3 imposes an upper limit on the magnitude of the feedback controller. The 30 dB upper limit is based on a separate experiment with 10 subjects, where each subject was asked to follow a single-frequency sinusoid using only error feedback (i.e., feedforward of the reference signal was not available). In this experiment, the peak magnitude of the feedback controller used by the subjects is approximately 30 dB, suggesting that 30 dB is the peak gain that a human can use in feedback. Condition C4 implies that the human's sensory feedback time delay is in the range of 80 ms to 500 ms. This is consistent with [7,62-64]. Since the sampling rate in this experiment for both groups is 20 ms, we assume that $\delta \in \{4, 5, \dots, 25\}$.

Appendix C. Numerical examples

We present two numerical examples using the SSID technique described in Section 3 and Appendix A. For both examples, the plant components are G(z) = 1/(z + 0.2) and $h^{-1}(x) = x - 0.4x^2 + 0.2x^3$. We numerically simulate the closed-loop system shown in Fig. 5 for a given feedback system $(d, G_{\rm fb})$ and feedforward system $(f, G_{\rm ff})$ where all initial conditions are zero. The numerical simulations yield data signals r_k and v_k , which are used to compute best-fit models $(d^+, G_{\rm fb}^+)$ and $(f^+, G_{\rm ff}^+)$.

Example 1. Consider d = 8, $G_{\text{fb}}(z) = 0.43/(z - 0.31)$, $G_{\text{ff}}(z) = (3z - 6)/z$ and $\alpha = [-0.50.1 \ 0 \ 0]^{\text{T}}$. Let $n_{\text{ff}} = 1$ and define the candidate pools

$$\begin{split} \Gamma_{1} &\triangleq \{ \gamma \in \mathbb{R}^{3} : e_{1}\gamma, e_{2}\gamma \in \{-1 + 0.25\tau\}_{\tau=0}^{8}, \\ &e_{3}\gamma \in \{4 + \tau\}_{\tau=0}^{21}\}, \\ \Gamma_{2} &\triangleq \{ \gamma \in \mathbb{R}^{3} : e_{1}\gamma, e_{2}\gamma \in \{-1 + 0.125\tau\}_{\tau=0}^{16}, \\ &e_{3}\gamma \in \{4 + \tau\}_{\tau=0}^{21}\}, \\ \Gamma_{3} &\triangleq \{ \gamma \in \mathbb{R}^{3} : e_{1}\gamma, e_{2}\gamma \in \{-1 + 0.0625\tau\}_{\tau=0}^{32}, \\ &e_{3}\gamma \in \{4 + \tau\}_{\tau=0}^{21}\}. \end{split}$$

Journal of the Franklin Institute xxx (xxxx) xxx

where $e_1 \triangleq [1 \ 0 \ 0]$, $e_2 \triangleq [0 \ 1 \ 0]$, and $e_3 \triangleq [0 \ 0 \ 1]$. The candidate pools define candidate pairs (d, G_{fb}) . All 3 candidate pools have the same boundaries, but Γ_3 has more elements than Γ_2 , and Γ_2 has more elements than Γ_1 . Note G_{fb} is not a member of the candidate pool, and thus the identification cannot yield the exact controller components. This example demonstrates how increasing the density of the candidate pool yields more accurate identifications.

For each of the 3 candidate pools, the SSID algorithm in Section 4 is used to obtain d^+ , $G_{\rm fb}^+$, $G_{\rm ff}^+$, and α^+ .

For Γ_1 , the SSID yields $d^+ = 8$, $G_{\rm fb}^+ = 0.5/(z - 0.25)$, $G_{\rm ff}^+ = (3.62z - 6.73)/z$, and $\alpha^+ = [-0.49527 \ 0.09407 \ 0.00195 \ 0.00016]^{\rm T}$.

For Γ_2 , the SSID yields $d^+ = 8$, $G_{\rm fb}^+ = 0.375/(z - 0.375)$, $G_{\rm ff}^+ = (2.78z - 5.71)/z$, and $\alpha^+ = [-0.50342 \ 0.10411 \ -0.00102 \ -0.00023]^{\rm T}$.

For Γ_3 , the SSID yields $d^+ = 8$, $G_{\rm fb}^+ = 0.4375/(z - 0.3125)$, $G_{\rm ff}^+ = (3.25z - 6.28)/z$, and $\alpha^+ = [-0.49891 \ 0.09855 \ 0.00065 \ -0.00002]^{\rm T}$.

Example 2. Consider the same parameters of the previous example, except $G_{\rm ff}(z) = 2/(5z + 2)$ and $n_{\rm ff} = 2$. Thus, $G_{\rm ff}$ is IIR, and we approximate $G_{\rm ff}$ by a second-order FIR.

For Γ_1 , the SSID yields $d^+ = 8$, $G_{\rm fb}^+ = 0.5/(z - 0.25)$, $G_{\rm ff}^+ = (0.30z^2 - 0.20z + 0.16)/z^2$, and $\alpha^+ = [-0.54127, 0.10708, -0.00066, 0.00026]^{\rm T}$.

For Γ_2 , the SSID yields $d^+ = 8$, $G_{\rm fb}^+ = 0.375/(z - 0.375)$, $G_{\rm ff}^+ = (-0.26z^2 + 0.89z - 0.33)/z^2$, and $\alpha^+ = [-0.48117, 0.09672, 0.00056, -0.00016]^{\rm T}$.

For Γ_3 , the SSID yields $d^+ = 8$, $G_{\rm fb}^+ = 0.4375/(z - 0.3125)$, $G_{\rm ff}^+ = (0.04z^2 + 0.31z - 0.07)/z^2$, and $\alpha^+ = [-0.51228, 0.10208, -0.00003, 0.00005]^{\rm T}$.

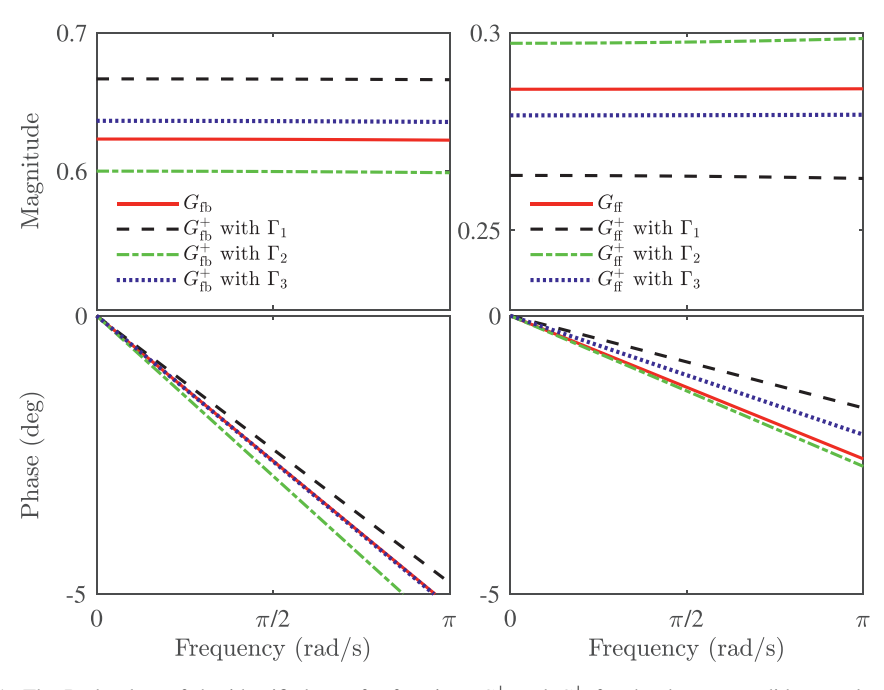


Fig. C.1. The Bode plots of the identified transfer functions G_{fb}^+ and G_{ff}^+ for the densest candidate pool Γ_3 results in the best estimates of G_{fb} and G_{ff} .

Journal of the Franklin Institute xxx (xxxx) xxx

Fig. C.1 shows the Bode plots of the identified transfer functions for each of the 3 candidate pools. The Bode plots of G_{fb}^+ and G_{ff}^+ are closest to G_{fb} and G_{ff} for the candidate pool Γ_3 , which is denser than Γ_1 and Γ_2 .

Appendix D. Validation of SSID Results

To validate the SSID results, for each trial we use the identified control pairs $(d^+, G_{\rm fb}^+)$ and $(f^+, G_{\rm ff}^+)$ to simulate the closed-loop system, where the input to the simulation is $\{r_k\}_{k=1}^{N_s}$, the output of the simulation is the validation data $\{y_k^+\}_{k=1}^{N_s}$, and all initial conditions are zero. We then use the experimental data $\{y_k\}_{k=1}^{N_s}$ and validation data $\{y_k^+\}_{k=1}^{N_s}$ to calculate the variance accounted for (VAF) for each trial. VAF is a measure of the accuracy of the identified controllers and is given by

VAF
$$\triangleq 1 - \frac{\sum_{k=1}^{N_s} |y_k - y_k^+|^2}{\sum_{k=1}^{N_s} |y_k|^2}.$$

Fig. D.1 shows the mean and standard deviation of VAF for each trial. For both groups, the mean VAF increases and the standard deviation decreases over the 40 trials. The increase in the VAF suggests that the identified models obtained for the later trials are a more accurate representation of the data than the models obtained for the earlier trials. This means that as the subjects learn, their control behavior can be better modeled by the control structure used in this paper.

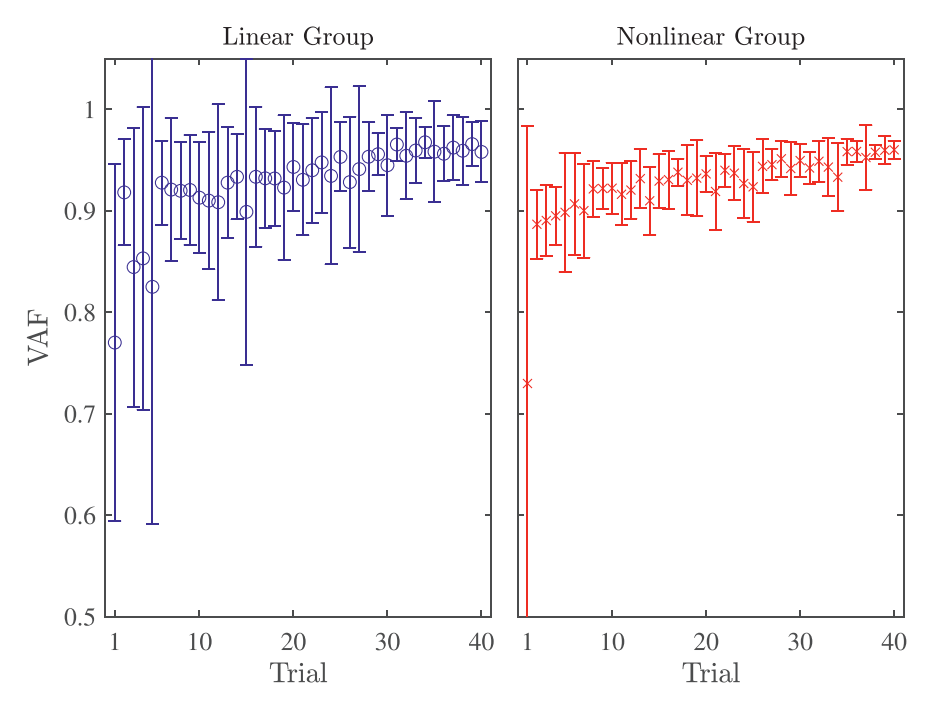


Fig. D.1. Mean and standard deviation of VAF on each trial. For both experiments, the mean VAF increases over the 40 trials. The symbols \circ and \times indicate the mean of the 11 subjects for linear and nonlinear experiments respectively and the vertical lines show one standard deviation above and below the mean.

JID: FI [m1+;February 20, 2021;4:13]

S. Koushkbaghi, J.B. Hoagg and T.M. Seigler

Journal of the Franklin Institute xxx (xxxx) xxx

CRediT authorship contribution statement

Sajad Koushkbaghi: Conceptualization, Methodology, Software, Formal analysis, Investigation, Writing - original draft. **Jesse B. Hoagg:** Conceptualization, Writing - review & editing, Funding acquisition. **T. Michael Seigler:** Conceptualization, Project administration, Supervision, Validation, Writing - review & editing, Funding acquisition.

References

- [1] D. McRuer, D.H. Weir, Theory of manual vehicular control, IEEE Trans. Man-Mach. Syst. 10 (4) (1969) 257–291.
- [2] G. Burnham, Jinbom Seo, G. Bekey, Identification of human driver models in car following, IEEE Trans. Autom. Control 19 (6) (1974) 911–915.
- [3] R. Hess, J.K. Moore, M. Hubbard, Modeling the manually controlled bicycle, IEEE Transactions on Systems, Man, and Cybernetics - Part A: Systems and Humans 42 (3) (2012) 545–557.
- [4] M. Mulder, A. Abbink, E.R. Boer, F.M. Drop, K. van der El, M.M. Paasen, Manual control cybernetics: state-of-the-art and current trends, IEEE Trans. Hum. Mach. Syst. 48 (5) (2018) 468–485.
- [5] A. Tustin, The nature of the operator's response in manual control, and its implications for controller design, J. Inst. Electr. Eng. - Part IIA: Autom. Regul. Servo Mech. 94 (2) (1947) 190–206.
- [6] D.T. McRuer, E.S. Krendel, The human operator as a servo system element, J. Frankl. Inst. 267 (5) (1959) 381–403.
- [7] D. Mcruer, D. Graham, E. Krendel, W. Reisener, Human pilot dynamics in compensatory systems: theory, models, and experiments with controlled element and forcing function variations, Air Force Flight Dynamics Laboratory, Research and Technology Division, Air Force Systems Command, Wright-Patterson Air Force Base, 1965. Technical Report AFFDL-TR-65-15
- [8] D.T. McRuer, H.R. Jex, A review of quasi-linear pilot models, IEEE Trans. Hum. Factors Electron. HFE-8 (3) (1967) 231–249.
- [9] D.T. McRuer, E.S. Krendel, Mathematical models of human pilot behavior, AGARDograph No. 188. (1974).
- [10] D.T. McRuer, L.G. Hofmann, H.R. Jex, G.P. Moore, A.V. Phatak, D.H. Weir, J. Wolkovitch, New approaches to human-pilot/vehicle dynamic analysis, Air Force Flight Dynamics Laboratory, Tech. Rep. AFFDL-TR-67-150, 1968.
- [11] M. Ito, Neurophysiological aspects of the cerebellar motor control system, Int. J. Neurol. 7 (1970) 162–176.
- [12] R.A. Schmidt, A schema theory of discrete motor skill learning, Psychol. Rev. 82 (1975) 225–260.
- [13] P. Neilson, M. Neilson, N. O'dwyer, Internal models and intermittency: a theoretical account of human tracking behavior, Biol. Cybern. 58 (2) (1988) 101–112.
- [14] M. Kawato, Internal models for motor control and trajectory planning, Curr. Opin. Neurobiol. 9 (1999) 718–727.
- [15] H. Gomi, M. Kawato, The cerebellum and VOR/OKR learning models, Trends Neurosci. 15 (1992) 445-453.
- [16] C. Tin, C. Poon, Internal models in sensorimotor integration: perspectives from adaptive control theory, J. Neural Eng. 2 (2005) S147–S163.
- [17] R. Shadmehr, M.A. Smith, J.W. Krakauer, Error correction, sensory prediction, and adaptation in motor control, Ann. Rev. Neurosci. 33 (1) (2010) 89–108.
- [18] M. Kawato, A hierachical neural-network model for control and learning of voluntary movement, Biol. Cybern. 57 (1987) 169–185.
- [19] P. Neilson, N. O'dwyer, M. Neilson, Stochastic prediction in pursuit tracking: an experimental test of adaptive model theory, Biol. Cybern. 58 (2) (1988) 113–122.
- [20] H. Gomi, M. Kawato, Learning control for a closed loop system using feedback-error-learning, in: Proceedings of the 29th IEEE Conference on Decision and Control, IEEE, 1990, pp. 3289–3294.
- [21] M.I. Jordan, D.E. Rumelhart, Forward models: supervised learning with a distal teacher, Cogn. Sci. 16 (1992) 307–354.
- [22] M. Kawato, H. Gomi, A computational model of four regions of the cerebellum based on feedback-error learning, Biol. Cybern. 68 (1992) 95–103.
- [23] P.D. Neilson, M.D. Neilson, N.J. O'Dwyer, What limits high speed tracking performance? Hum. Mov. Sci. 12 (1-2) (1993) 85–109.
- [24] R.C. Miall, D.M. Wolpert, Forward models for physiological motor control, Neural Netw. 9 (1996) 1265–1297.

JID: FI [m1+;February 20, 2021;4:13]

S. Koushkbaghi, J.B. Hoagg and T.M. Seigler

Journal of the Franklin Institute xxx (xxxx) xxx

- [25] D.M. Wolpert, R.C. Miall, M. Kawato, Internal models in the cerebellum, Trends Cogn. Sci. (Regul. Ed.) 2 (1998) 338–347.
- [26] R. Shadmehr, F.A. Mussa-Ivaldi, Adaptive representation of dynamics during learning of a motor task, J. Neurosci. 14 (1994) 3208–3224.
- [27] M.A. Smith, J. Brandt, R. Shadmehr, Motor disorder in Huntington's disease begins as a dysfunction in error feedback control, Nature 403 (6769) (2000) 544.
- [28] M. Haruno, D.M. Wolpert, M. Kawato, Advances in Neural Information Processing Systems, MIT Press, pp. 31–37
- [29] D.A. Nowak, J. Hermsdorfer, S. Glasauer, L. Meyer, N. Mai, The effects of digital anaesthesia on predictive grip force adjustments during vertical movements of a grasped object, Eur. J. Neurosci. 14 (2001) 756–762.
- [30] D.A. Nowak, S. Glasauer, L. Meyer, N. Mai, J. Hermsdorfer, The role of cutaneous feedback for anticipatory grip force adjustments during object movements and externally imposed variation of the direction of gravity, Somatosens. Motor Res. 19 (2002) 49–60.
- [31] O. Bock, Early stages of load compensation in human aimed arm movements, Behav. Brain Res. 55 (1993) 61–68.
- [32] J.R. Flanagan, A.M. Wing, Modulation of grip force with load force during point-to-point movements, Exp. Brain Res. 95 (1993) 131–143.
- [33] J.R. Flanagan, J.R. Tresilian, A.M. Wing, Coupling of grip force and load force during arm movements with grasped objects, Neurosci. Lett. 152 (1993) 53–56.
- [34] J.R. Flanagan, J.R. Tresilian, Grip-load force coupling: a general control strategy for transporting objects, J. Expe. Psychol.: Hum. Percept. Perform. 20 (1994) 944–957.
- [35] D.M. Wolpert, Z. Ghahramani, M.I. Jordan, An internal model for sensorimotor integration, Science 269 (1995) 1880–1882.
- [36] D.L. Weeks, M.-P. Aubert, A.G. Feldman, M.F. Levin, One-trial adaptation of movement to changes in load, J. Neurophysiol. 75 (1996) 60–74.
- [37] F. Gandolfo, F.A. Mussa-Ivaldi, E. Bizzi, Motor learning by field approximation, Proc. Natl. Acad. Sci. 93 (1996) 3843–3846.
- [38] S.J. Goodbody, D.M. Wolpert, Temporal and amplitude generalization in motor learning, J. Neurophysiol. 79 (1998) 1825–1838.
- [39] C.G. Atkeson, Learning arm kinematics and dynamics, Ann. Rev. Neurosci. 12 (1989) 157-183.
- [40] J. Diedrichsen, T. Verstynen, A. Hon, Y. Zhang, R.B. Ivry, Illusions of force perception: the role of sensori-motor predictions, visual information, and motor errors, J. Neurophysiol. 97 (2007) 3305–3313.
- [41] X. Zhang, S. Wang, J.B. Hoagg, T.M. Seigler, The roles of feedback and feedforward as humans learn to control unknown dynamic systems, IEEE Trans. Cybern. 48 (2) (2018) 543–555.
- [42] A.J.S. Sheffler, S.A.S. Mousavi, E. Hellström, M. Jankovic, M.A. Santillo, T.M. Seigler, J.B. Hoagg, Effects of reference-command preview as humans learn to control dynamic systems, in: Proceedings of the 2019 IEEE International Conference on Systems, Man and Cybernetics (SMC), 2019, pp. 4199–4204.
- [43] K. van der El, D.M. Pool, H.J. Damveld, M.R.M. van Paassen, M. Mulder, An empirical human controller model for preview tracking tasks, IEEE Trans. Cybern. 46 (11) (2016) 2609–2621.
- [44] X. Zhang, T.M. Seigler, J.B. Hoagg, The impact of nonminimum-phase zeros on human-in-the-loop control systems, IEEE Trans. Cybern. doi:10.1109/TCYB.2020.3027502.
- [45] J.R. Flanagan, A.K. Rao, Trajectory adaptation to a nonlinear visuomotor transformation: evidence of motion planning in visually perceived space, J. Neurophysiol. 74 (5) (1995) 2174–2178.
- [46] P.R. Davidson, R.D. Jones, H.R. Sirisena, J.H. Andreae, Detection of adaptive inverse models in the human motor system, Hum. Mov. Sci. 19 (5) (2000) 761–795.
- [47] A. Ghous, P.D. Neilson, Evidence for internal representation of a static nonlinearity in a visual tracking task, Hum. Mov. Sci. 21 (5) (2002) 847–879.
- [48] H. Heuer, M. Hegele, Learning new visuo-motor gains at early and late working age, Ergonomics 50 (7) (2007) 979–1003.
- [49] H. Heuer, M. Hegele, Adaptation to a nonlinear visuomotor amplitude transformation with continuous and terminal visual feedback., J. Mot. Behav. 40 (5) (2008) 368–379.
- [50] W.B. Verwey, H. Heuer, Nonlinear visuomotor transformations: locus and modularity, Q. J. Exp. Psychol. 60 (12) (2007) 1629–1659.
- [51] M. Rieger, W.B. Verwey, C. Massen, The effect of continuous, nonlinearly transformed visual feedback on rapid aiming movements, Exp. Brain Res. 191 (1) (2008) 1.
- [52] X. Zhang, S. Wang, T.M. Seigler, J.B. Hoagg, A subsystem identification technique for modeling control

JID: FI [m1+;February 20, 2021;4:13]

S. Koushkbaghi, J.B. Hoagg and T.M. Seigler

Journal of the Franklin Institute xxx (xxxx) xxx

- strategies used by humans, in: Proceedings of the American Control Conference (ACC), Portland, OR, 2014, pp. 2827–2832.
- [53] X. Zhang, T.M. Seigler, J.B. Hoagg, Modeling the control strategies that humans use to control nonminimum-phase systems, in: Proceedings of the 2015 American Control Conference (ACC), 2015, pp. 471–476.
- [54] X. Zhang, J.B. Hoagg, Subsystem identification of multivariable feedback and feedforward systems, Automatica 72 (2016) 131–137.
- [55] S.A.S. Mousavi, X. Zhang, T.M. Seigler, J.B. Hoagg, Characteristics that make dynamic systems difficult for a human to control, in: Proceedings of the 2016 American Control Conference (ACC), 2016, pp. 4391–4396.
- [56] I. Gustavsson, L. Ljung, T. Söderström, Identification of processes in closed loop—identifiability and accuracy aspects, Automatica 13 (1) (1977) 59–75.
- [57] U. Forssell, L. Ljung, Closed-loop identification revisited, Automatica 35 (7) (1999) 1215–1241.
- [58] R. Isermann, M. Münchhof, Identification of dynamic systems: an introduction with applications, Springer Science & Business Media, 2010.
- [59] F.M. Drop, D.M. Pool, M.R.M. van Paassen, M. Mulder, H.H. Bülthoff, Objective model selection for identifying the human feedforward response in manual control, IEEE Trans. Cybern. 48 (1) (2018) 2–15.
- [60] F. Chang, R. Luus, A noniterative method for identification using Hammerstein model, IEEE Trans. Autom. Control 16 (5) (1971) 464–468.
- [61] W.M. Haddad, D.S. Bernstein, Explicit construction of quadratic Lyapunov functions for the small gain, positivity, circle, and popov theorems and their applications to robust stability. part II: discrete-time theory, Int. J. Robust Nonlinear Control 4 (1994) 249–265.
- [62] A. Abdel-Malek, V.Z. Marmarelis, Modeling of task-dependent characteristics of human operator dynamics pursuit manual tracking, IEEE Trans. Syst. Man Cybern. 18 (1) (1988) 163–172.
- [63] K. Amano, N. Goda, S. Nishida, Y. Ejima, T. Takeda, Y. Ohtani, Estimation of the timing of human visual perception from magnetoencephalography, J. Neurosci. 26 (15) (2006) 3981–3991.
- [64] J.-J. O. de Xivry, P. Lefèvre, Saccades and pursuit: two outcomes of a single sensorimotor process., J. Physiol. (Lond.) 584 (2007) 11–23. Pt 1